Molecular Therapy
Nucleic Acids
Original Article

In vivo genome editing using 244-*cis* LNPs and low-dose AAV achieves therapeutic threshold in hemophilia A mice

Jeong Pil Han,[1,6] Yeji Lee,[2,6] Jeong Hyeon Lee,[1] Hye Yoon Chung,[1] Geon Seong Lee,[1] Yu Ri Nam,[3] Myeongjin Choi,[4] Kyoung-Sik Moon,[4] Haeshin Lee,[3] Hyukjin Lee,[2] and Su Cheong Yeom[1,5]

[1]Graduate School of International Agricultural Technology and Institute of Green BioScience and Technology, Seoul National University, Pyeongchang, Gangwon 25354, Korea; [2]College of Pharmacy, Graduate School of Pharmaceutical Sciences, Ewha Womans University, Seodaemun-gu, Seoul 03760, Korea; [3]Deartment of Chemistry, Korea Advanced Institute of Science and Technology (KAIST), Yuseong-gu, Daejeon 34141, Korea; [4]Department of Advanced Toxicology Research, Korea Institute of Toxicology, Yuseong-gu, Daejeon 34114, Korea; [5]WCU Biomodulation Major, Department of Agricultural Biotechnology, Seoul National University, Gwanank-gu, Seoul 08826, Korea

Gene therapy and rebalancing therapy have emerged as promising approaches for treating hemophilia A, but there are limitations, such as temporary efficacy due to individual differences. Genome editing for hemophilia has shown long-term therapeutic potential in preclinical trials. However, a cautious approach is necessary because genome editing is irreversible. Therefore, we attempted to induce low-level human factor 8 (hF8) gene knockin (KI) using 244-*cis* lipid nanoparticles and low-dose adeno-associated virus to minimize side effects and achieve a therapeutic threshold in hemophilia A mice. We selected the serpin family C member 1, *SerpinC1*, locus as a target to enable a combined rebalancing strategy with h*F8* KI to augment efficacy. This strategy improved blood coagulation activity and reduced hemophilic complications without adverse effects. Furthermore, hemophilic mice with genome editing exhibit enhanced survival for 40 weeks. Here, we demonstrate an effective, safe, and sustainable treatment for hemophilia A. This study provides valuable information to establish safe and long-term genome-editing-mediated treatment strategies for treating hemophilia and other protein-deficient genetic diseases.

INTRODUCTION

Hemophilia A, a coagulation disorder, is caused by a deficiency of the coagulation factor 8 (FVIII) protein resulting from a genetic defect in coagulation factor 8 (*F8*) and is prevalent in 1 of 5,000 males.[1] Prophylaxis is the most common treatment strategy for hemophilia and involves the intravenous administration of deficient clotting factors to maintain appropriate levels of these coagulation factors.[2] However, recombinant FVIII (rFVIII) has a short half-life, with an average of 12 h,[3] and patients with hemophilia A are typically required to inject rFVIII every 2 days.[4] To date, efforts to extend the half-life of rFVIII have been limited, with an average half-life of 18 h.[3] Additionally, rFVIII administration can lead to the development of FVIII inhibitors in approximately 30% of patients with hemophilia A after treatment.[5] The acquisition of FVIII inhibitors is a significant limitation of prophylaxis therapy using rFVIII, rendering replacement therapy ineffective, thereby increasing the risk of bleeding and leading to an early onset of progressive arthropathy.[6,7] Therefore, there is a pressing need to develop new treatments to address the short-lasting therapeutic effects and the risk of inhibitor development associated with rFVIII therapy for hemophilia A.

Next-generation treatment strategies for hemophilia A, such as gene therapy and rebalancing therapy, are under clinical trials.[8,9] Gene therapy includes an *ex vivo* strategy that integrates a protein-coding sequence into the host chromosome of a cell and delivers it to the body and an *in vivo* strategy that directly delivers genetic material to the body.[10] Adeno-associated virus (AAV) is a viral vector commonly used for *in vivo* gene therapy owing to its low immunogenicity, serotype-specific tropism, and low-integration characteristics.[8] A single administration of AAV shows a long-lasting therapeutic effect for several months to years. Global pharmaceutical companies, including BioMarin, Sangamo, Sanofi, and Spark, are conducting clinical trials for AAV-mediated gene therapies for hemophilia A with ongoing developments.[8] However, a clinical trial reported a 43% decrease in human FVIII (hFVIII) expression within 2 years of AAV transduction.[11] Repeated AAV transduction may be required, but it could reduce the therapeutic effect owing to the production of neutralizing antibodies against the AAV capsid.[12]

Rebalancing therapy restores the blood-clotting ability by downregulating the anticoagulant pathway and can be applied to patients with

Received 25 May 2023; accepted 4 October 2023;
https://doi.org/10.1016/j.omtn.2023.102050.

[6]These authors contributed equally

Correspondence: Hyukjin Lee, PhD, Professor, College of Pharmacy, Ewha Womans University, 52 Ewhayeodae-gil, Seodaemun-gu, Seoul 03760, Korea.
E-mail: hyukjin@ewha.ac.kr
Correspondence: Su Cheong Yeom, DVM, PhD, Professor, Graduate School of International Agricultural Technology, Seoul National University, 1447 Pyeongchang-Ro, Daewha, Pyeongchang, Gangwon 25354, Korea.
E-mail: scyeom@snu.ac.kr

hemophilia A and B with inhibitors.[13] Tissue factor pathway inhibitor, activated protein C, and serpin family C member 1 (*SerpinC1*) have been studied as candidate targets for rebalancing therapy.[14–16] *SerpinC1* encodes antithrombin (AT), which inhibits thrombin generation and is a promising target for rebalancing therapies. Fitusiran, a small interfering RNA for hemophilia treatment targeting *SerpinC1*, decreased bleeding episodes in clinical trials.[16] However, fitusiran was ineffective in restoring activated partial thromboplastin time (aPTT), indicating an insufficient hemostatic effect on acute bleeding, such as trauma[17]; therefore, an additional recombinant clotting factor should be used.

Genome editing is a valid option for effective hemophilia treatment as it restores the ability to produce endogenous blood-clotting factors. The ribonucleoprotein (RNP) complex of clustered regularly interspaced short palindromic repeats (CRISPR)-CRISPR-associated protein 9 (CRISPR-Cas9) and a single guide RNA (sgRNA) induces targeted double-stranded DNA breakage (DSB). Therapeutic gene knockin (KI) is feasible using a DNA repair mechanism that generates CRISPR-Cas9-mediated DSB and provides an appropriate donor template.[18] The KI of the FVIII coding sequence can be applied universally to patients with different variants of hemophilia A. The therapeutic gene KI alleviates coagulopathy in hemophilia A and B mice.[19,20] For therapeutic gene KI in a mouse model, multiple AAVs have been used to encode the Cas9 protein, sgRNA, and donor templates.[20,21] The application of dual or triple AAVs can cause transduction interference,[21] which contributes to low KI efficiency[22,23] and increases the total amount of AAV administered, potentially increasing side effects. High-dose AAV transduction can induce an immune response, and there have been cases of patient death in clinical trials.[24,25] In addition, the risk of transgene integration into the host chromosome using AAV vectors is constantly raised.[26] Therefore, to develop an *in vivo* therapeutic gene, KI, it is necessary to minimize the AAV dose and discover alternative delivery tools for CRISPR-Cas9 and donor templates.

Lipid nanoparticles (LNPs) are a non-viral delivery option that can deliver genetic material to different target organs based on their formulation and show lower immunogenicity than viral vectors.[27] They mediate the targeted delivery of Cas9 mRNA and sgRNA to the cytosol. After Cas9 protein synthesis on ribosomes, the nucleus-localizing signal on the Cas9 protein enables the movement of the Cas9 RNP complex into the nucleus via the nuclear pore complex. The Cas9 RNP produced after LNP-mediated delivery of Cas9 mRNA and sgRNA rapidly degrades within a few days,[28] reducing the likelihood of undesirable events such as off-target DSB formation or immune response. Our previous study demonstrated the safe and sustainable rebalancing of therapeutic effects of *Serpinc1* targeting using LNP-encapsulated *Streptococcus pyogenes* Cas9 (SpCas9) mRNA.[19] This study used a novel engineered 244-*cis* LNP that induces lower immune responses than the responses evoked by previously used LNPs. The 244-*cis* ionizable lipid has been developed for the targeted *in vivo* delivery of mRNA therapeutics; its unique characteristics such as minimal immune stimulation upon systemic administration as well as the feasibility of repeat doses of mRNA/LNP without losing potency have been highlighted.[29]

This study aimed to develop a hemophilia A therapy through human *F8* (h*F8*) KI into the *Serpinc1* locus, utilizing a combination of LNP and AAV as a genetic material delivery tool. The traditional goal of prophylaxis therapy has been specified as a blood concentration of FVIII greater than 1% of the normal levels, and a recent clinical study suggested that it needs to be set between 8% and 12% for effective prophylaxis.[30] Thus, even low levels of FVIII induced by an inefficient therapeutic gene KI could remain valid and efficacious for hemophilia A treatment. Therefore, we attempted to achieve a low therapeutic threshold using low-dose AAV and 244-*cis* LNP. Our results demonstrate a sustainable, safe, and effective gene therapy for hemophilia A combining *Serpinc1* targeting and h*F8* KI using viral and non-viral vectors.

RESULTS

AAV-donor and liver-specific 244-*cis* LNP

The h*F8* gene (accession no. NM_000132) encodes the hFVIII protein, which comprises A1-A2-B-A3-C1-C2 domains. The h*F8* coding sequence spans 7.1 kb, exceeding the payload capacity of AAV vectors. The B-domain of hFVIII can be removed without compromising the FVIII function, and B-domain-deleted hFVIII (hFVIII-BDD) has been utilized for rFVIII production.[31] This study aimed to establish an h*F8* KI in the *SerpinC1* locus of hemophilia A mouse liver cells. Splicing acceptor sequences were incorporated to employ the endogenous promoter signal of *SerpinC1*, and the 4,314-base pair (bp) hFVIII-BDD coding sequence was packed in the AAV-donor template. Additionally, we applied a homology-mediated end-joining (HMEJ) strategy, which combines homology-independent targeted integration (HITI) and homology-directed repair (HDR) to enhance the efficiency of *in vivo* KI.[32] The sgRNA sequences were designated as 5′-TGTGCATTTACCGCTCCCCTGGG-3′, located in the third exon of the *SerpinC1* gene. The 70-bp homology arms and the sgRNA sequences were positioned at both ends of the donor template (Figure 1A). The AAV serotype 8 (AAV8) was used as a tool for donor delivery in our previous *in vivo* therapeutic KI study.[21] After verifying liver tropism in a luciferase (Luc) transduction experiment (Figure 1B), AAV8 was selected as the h*F8* vector for donor delivery (AAV-donor).

The LNPs used in this study included the ionizable lipid 244-*cis*. This ionizable lipid contained three ester structures and three unsaturated bonds based on a piperazine heterocyclic structure (Figure 1C). In the microfluidic system, phospholipids, e.g., dioleylphosphatidyl ethanolamine, polyethylene glycol (PEG) lipids, e.g., C16-PEG2000 ceramide, cholesterol, and ionizable lipids, were introduced on one side, and SpCas9 mRNA and sgRNA were loaded at a 1:1 (w/w) ratio on the other side. The LNPs were formulated by flowing both solutions at a constant rate (12 mL/min). In a previous study, 7.0 mM citrate with 20 mM NaCl was used as a buffer for SpCas9 mRNA and sgRNA, using a pH 5.0 condition (higher than the common condition of pH 3) to increase ionic strength.[19] We adopted this buffer

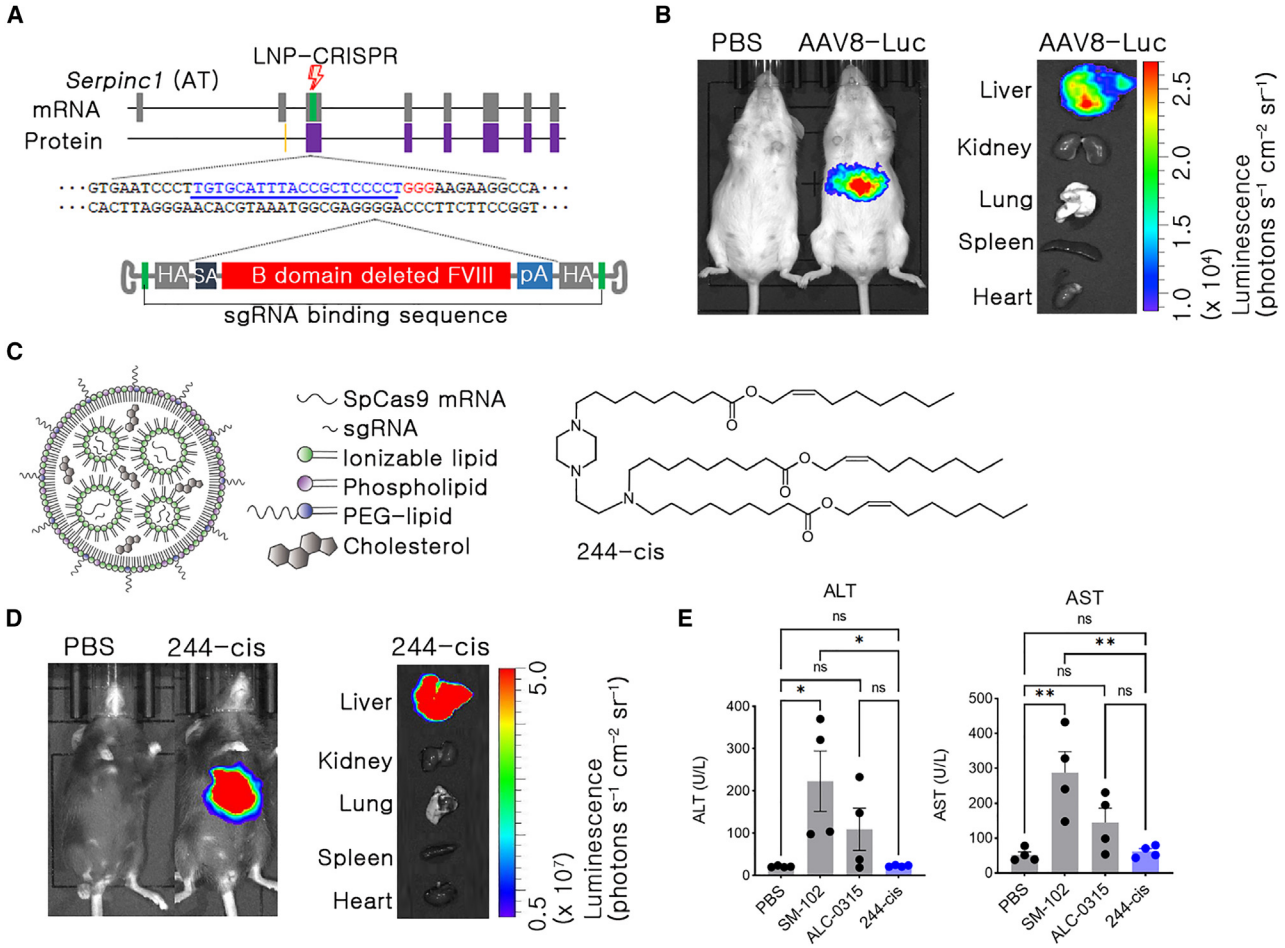

Figure 1. Adeno-associated virus (AAV) vectors and lipid nanoparticles (LNPs) were prepared for liver-targeted *in vivo* genome editing

(A) Schematic representation of *in vivo* human B-domain-deleted *F8* KI in the third exon of *SerpinC1*. Thunder symbol, DSB site; blue letters, sgRNA binding sequences; red letters, protospacer adjacent motif sequences; HA, homology arm; SA, splicing acceptor; pA, polyadenylation; LNP-CRISPR, Lipid nanoparticle packed SpCas9 mRNA and sgRNA. (B) The biodistribution of AAV vectors in the body was analyzed by *in vivo* bioluminescence imaging using 1×10^{12} vector genomes per kilogram of body weight (vg/kg) of luciferase-encoded AAV serotype 8 (AAV8-Luc). Two weeks after AAV8-Luc transduction, a luminescent signal was detected in live mice and their organs. (C) Schematic of 244-*cis* LNP. LNP encapsulating SpCas9 mRNA and sgRNA comprised four lipids, including ionizable lipids. 244-*cis* ionizable lipid contains three ester structures and three unsaturated bonds based on the piperazine heterocyclic structure. (D) The biodistribution of LNPs was analyzed by measuring luciferase signal intensity 6 h after intravenous injection of 0.1 mg/kg (mpk) of 244-*cis* LNP into C57BL/6 (B6, wild type; WT). (E) Serum aspartate aminotransferase (AST) and alanine transaminase (ALT) concentrations 24 h after the injection of WT mice with 2.0 mpk 244-*cis* LNP. Each dot represents data from an individual mouse and is presented as mean ± standard error of the mean (SEM) (n = 3 for each group).

condition. Consequently, LNPs with a high encapsulation efficiency of 96.5%, size of 79.84 ± 22.26 nm, and polydispersity index (PDI) of 0.074 ± 0.031 were formulated. The results of measuring the size of the 244-*cis* LNP encapsulated with Cas9 mRNA/gRNA using a Zeta sizer are presented in Table S1.

The 244-*cis* LNPs encapsulated with firefly Luc (fLuc) mRNA were used to examine the *in vivo* distribution of LNPs. Bioluminescence was observed using an *in vivo* imaging system (IVIS) 6 h after intravenous injection of a 0.1 mg/kg dose, with higher luminescence values observed in mice injected with 244-*cis* LNPs than in mice administered PBS. An *ex vivo* analysis of the liver, lungs, spleen, heart, and kidneys revealed that the liver showed the highest luminescence values. The 244-*cis* LNPs targeted the liver when administered systemically (Figure 1D). This observation is consistent with the currently understood mechanism that when LNPs are injected into the circulatory system, PEG lipids are uncoated, and the ApoE protein in the blood attaches to the surface of the LNPs, interacting with low-density lipoprotein receptors in hepatocytes.[33,34] As LNPs target the liver, we compared 244-*cis* LNPs with ALC-0315 and SM-102 LNPs used in the COVID-19 vaccine produced by Pfizer and Moderna. Aspartate aminotransferase (AST) and alanine transaminase (ALT) levels, which indicate liver toxicity, were compared at 24 h after a single administration of 2 mg/kg fLuc mRNA (Figure 1E). Compared

with the PBS group, the 244-*cis* group showed comparable values of AST and ALT, which were lower than those of the ALC-0315 and SM-102 groups. Therefore, hepatotoxicity could not be observed, despite administering a high dose of 244-*cis* LNP. The results of evaluating the fLuc mRNA expression efficiency, as well as gene editing efficacy and biodegradability of 244-*cis*, ALC-0315, and SM-102 have been presented in the supplementary data (Figures S1 and S2).

Two-week interval between low-dose AAV and LNP transfection for *in vivo* KI

This study utilized the C57BL/6.*F8* intron 22 inversion ($F8^{I22I}$) mice,[35] which mimic the most common and severe bleeding clinical phenotype in patients with hemophilia A. Targeted DSB and the delivery of donor templates are necessary to achieve KI. Providing donor templates to the nucleus before DSB formation is crucial for generating KI.[36,37] DNA template could not pass the nuclear pore complex efficiently,[36] and the liver consists mostly of non-dividing cells in the G0/G1 phase with intact nuclear pore complex.[38] Synthetic lipids efficiently deliver genetic materials into the cytosol, but do not efficiently deliver DNA templates into the cellular nucleus. AAV is a single-stranded DNA virus and could deliver its genome into the nucleus of dividing or non-dividing cells.[39] Therefore, we selected an AAV vector to deliver DNA templates into the nucleus for the generation of KI.

The AAV is a single-stranded DNA virus, converted into double-stranded DNA after transduction into the cell nucleus. Seven days after transduction, AAV was enriched in non-dividing cells.[40] Contrastingly, LNP exhibits prompt and vigorous translation within 1–2 days of administration.[28] Considering the kinetics of AAV and LNP, AAV transduction is required before the transfection of LNP encapsulated with Cas9 mRNA and sgRNA. Therefore, we placed a 2-week interval between AAV and LNP administration in the mice.

In addition, the dosages of AAV and LNP were considered. In our previous study, the insertion and deletion (indel) frequency was approximately 20% in hepatocytes without detectable side effects in three times repeated dosing with 1.2 mg/kg (mpk) LNP-CRISPR.[19] As we intended to reduce the number of LNP administrations, 1.5 mpk 244-*cis* LNP was administered once (Figure 2A). Additionally, a phase 3 clinical trial for gene therapy of human hemophilia A was conducted recently using a viral dose of 6×10^{13} vector genomes per kilogram (vg/kg) of body weight for the treatment[41] (ClinicalTrials.gov: NCT03370913). To lower the possibility of side effects, including immune response and random integration using AAV, we determined the AAV dose to be 1×10^{12} vg/kg (2.5×10^{10} vg/mouse), which is 60 times lower than that used in the clinical trial (Figure 2A).

Combined use of AAV and LNP-induced liver-specific SerpinC1 targeting and decreased blood at levels

The generation of indels at the *SerpinC1* locus using LNP-CRISPR was analyzed using polymerase chain reaction (PCR) and T7 endonuclease I (T7E1) analysis of liver tissues. Indels were not detected in the wild-type (WT), $F8^{I22I}$, and AAV-donor groups. There were 7.4% indels in the LNP-CRISPR group and approximately 30% indels in the AAV-donor and LNP-CRISPR combined groups (AAV-LNP). The AAV-LNP group developed an indel frequency nearly four times higher than that in the LNP-CRISPR group, despite administering the same amount of LNP-CRISPR (Figures 2B and S3). As AAV does not produce DSBs, we hypothesized that AAV donors interfere with the repair process after DSB formation using LNP-CRISPR and induce a relatively high indel frequency. Similarly, partial AAV sequences can be integrated into DSBs.[42]

A primary goal of this study was to downregulate the blood AT concentration by targeting the *Serpinc1* locus. Therefore, the high indel frequency in the AAV-LNP group was beneficial. The LNP-CRISPR and AAV-LNP groups showed decreased blood AT concentrations by 13% and 30%, respectively, compared with the F8I22I group (Figure 2C). Fitusiran clinical trials reported a gradual increase in thrombin generation by AT inhibition.[17] Thus, this downregulation of AT was expected to induce the recovery of thrombin generation. Additionally, indels were not detected in other organs, such as the heart, lungs, spleen, kidneys, and testes, indicating that LNP-CRISPR targeting was specific to and effective in the liver (Figure S4).

Human factor 8 gene KI recovered hFVIII production *in vivo*

The presence of KI induced by the AAV-donor at the DSB site of the *Serpinc1* locus was verified by PCR using the liver tissue. Only the AAV-LNP group exhibited KI in PCR result (Figure 2D). To accurately assess KI efficiency in the *SerpinC1* locus, droplet digital PCR (ddPCR) was conducted using the liver tissue. Similar to the KI PCR results, the ddPCR results were positive only in the AAV-LNP group (0.13%), and were not detected in the other groups (Figures 2D and S5).

As 70-bp homology arm sequences were placed at the 5′ and 3′ ends of the AAV-donor, both HITI and HDR could potentially occur. Sanger sequencing using the KI PCR amplicons revealed that all KIs at the 3′ end seemed to be caused by HITI, whereas KIs at the 5′ end were produced through different integration mechanisms underlying HITI (71%, 10 of 14), HDR (14%, 2 of 14), AAV-trap (7%, 1 of 14),[21] or through an unknown mechanism (Figures 2E and S6). The HMEJ strategy appeared to induce various types of KI; however, HITI was dominant. The directional characteristics of KI were not analyzed thoroughly in this study. However, we inferred that DNA fusion first occurred at the 3′ end through HITI, followed by fusion at the 5′ end. The KI was not detected in organs other than the liver in the AAV-LNP group (Figure S4), indicating that detectable KI was induced only in the liver, wherein sufficient amounts of the AAV-donor and LNP-CRISPR were delivered simultaneously.

The h*F8* KI in the liver leads to hFVIII production. Therefore, we conducted an enzyme-linked immunosorbent assay (ELISA) to verify the expression of hFVIII using liver and blood samples. The average concentration of hFVIII was 25 ng/mL in the liver lysate (1 mg) of the AAV-LNP group. However, two mice in the AAV-LNP group

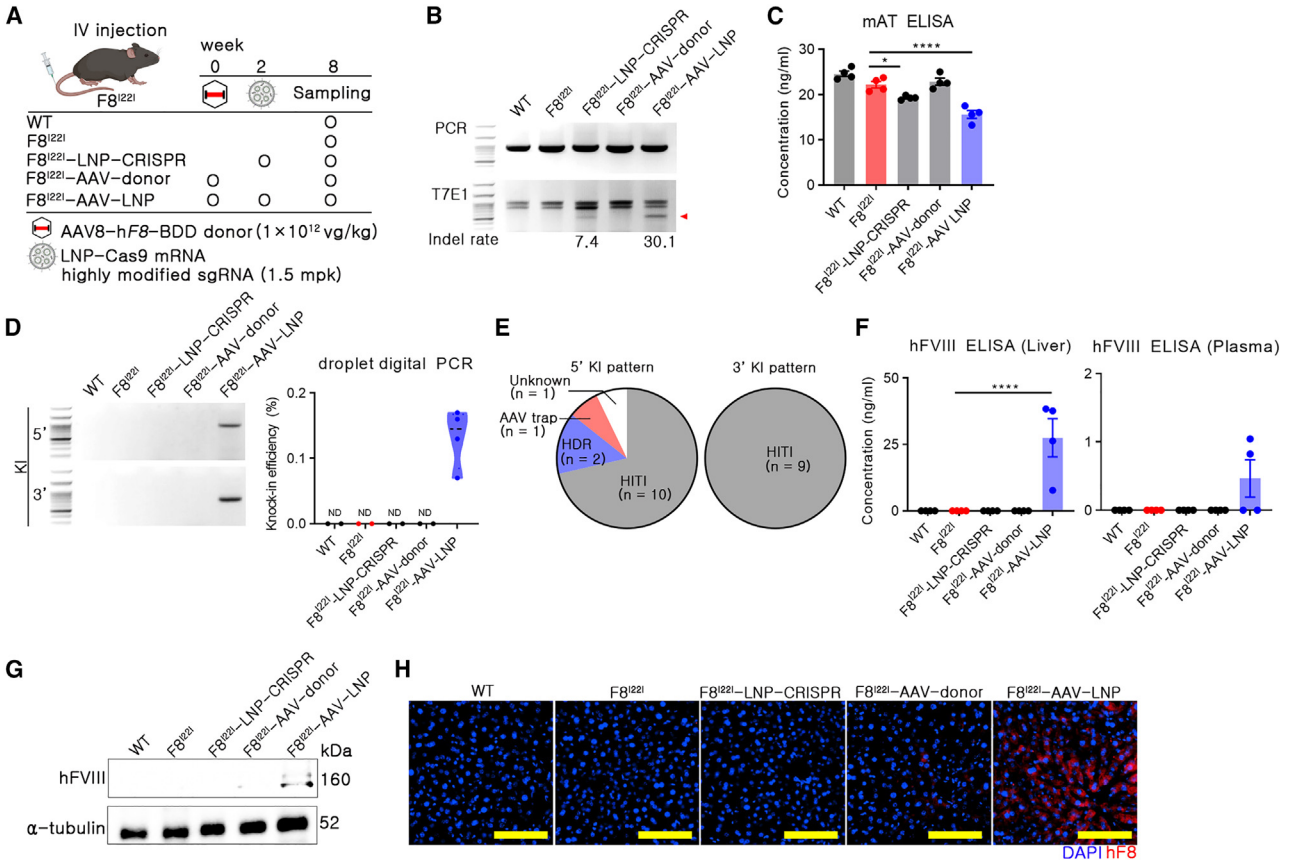

Figure 2. *In vivo* human factor 8 gene (h*F8*) knockin (KI) into the *SerpinC1* locus induced downregulation of mouse antithrombin (AT) and production of human factor 8 (hFVIII)

(A) A schematic displaying information on the experimental groups and injection schedules for genetic materials. IV, intravenous injection; $F8^{I22I}$, C57BL/6 mice *F8* intron 22 inversion. (B) Identification of insertions and deletions (indels) using T7E1 and indel rate calculation using image analysis. Red triangle: band cut by T7E1. (C) Mouse blood AT concentrations in each group were measured using an enzyme-linked immunosorbent assay (ELISA) (n = 4 per group). (D) PCR-based genotyping for the KI analysis. Primers were designed for both sides of the expected KI region (left). Droplet digital PCR (ddPCR) was conducted to analyze accurate KI efficiency in mouse liver tissues of the 8-week post-injection group (right; WT, $F8^{I22I}$, LNP-CRISPR, AAV-donor; n = 2; AAV-LNP; n = 4). (E) Sanger sequencing was conducted using 9–14 randomly selected clones from each KI-positive amplicon of $F8^{I22I}$-AAV-LNP. HITI: Homology-independent targeted integration. (F) Concentrations of hFVIII in the liver and blood were measured using ELISA (n = 4 for each group). (G) Western blotting for hFVIII and α-tubulin using liver tissue protein. (H) Immunofluorescence images showing liver hFVIII expression (100X). The yellow scale bar represents 200 μm. Statistical analyses were performed using one-way analysis of variance (ANOVA). Each dot represents data from an individual mouse and is presented as mean ± SEM. *$p < 0.05$, ****$p < 0.0001$.

showed low levels of hFVIII in the blood (Figure 2F). We reasoned that the hFVIII secreted into the bloodstream was consumed and remained at a lower concentration below the detectable range. Next, hFVIII synthesis in the liver was analyzed by western blotting, and an approximately 160-kDa anti-hFVIII antibody reactive band, consistent with the expected size of FVIII-BDD, was detected (Figure 2G). Immunofluorescence confirmed the expression of hFVIII in the liver tissue (Figure 2H).

Human factor 8 gene KI restored enhanced the coagulation phenotype in *in vitro* coagulation assays

Human patients with $F8^{I22I}$ hemophilia express nonfunctional FVIII with a truncation of the C-domain.[43] Similarly, $F8^{I22I}$ mice also produce FVIII but lack FVIII activity, which causes coagulopathy. Therefore, we assessed plasma concentrations of activated FVIII (FVIIIa) to determine whether therapeutic hFVIII improved blood coagulation. The plasma concentrations of FVIIIa were restored in the AAV-LNP group to approximately 10% of that in WT mice (Figure 3A). The production of FVIIIa could not be detected in the $F8^{I22I}$ control and LNP-CRISPR groups, but a small amount of FVIIIa was detected in the AAV-donor group, presumably because of random AAV integration or episomal expression promoted by the inverted terminal repeat (ITR) sequence.[44]

The final goal of hemophilia therapy is to re-establish coagulation capabilities. The aPTT test and calibrated automated thrombogram (CAT) could be utilized to analyze the hemostatic function and assess the recovery of coagulation activity for a combination of rebalancing

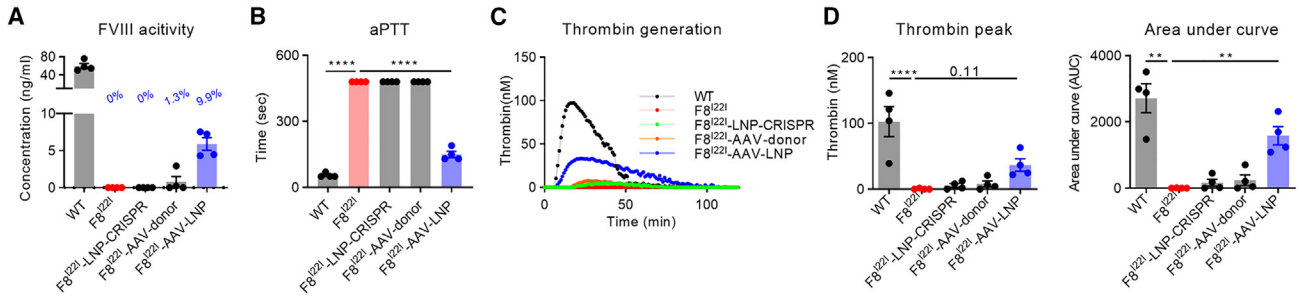

Figure 3. Combination of rebalancing therapy and hFVIII production improved coagulation activity

(A) Factor VIII activity (FVIIIa) in the plasma was measured through chromogenic analysis of the 8-week post-injection group (n = 4 for each group). The ratio values of FVIIIa were calculated by comparison with the mean value from the WT and are shown in blue text. (B) The coagulation activity in each group was analyzed based on activated partial thromboplastin time analysis (aPTT) (n = 4 for each group). (C) The thrombin generation potential was analyzed using a calibrated automated thrombogram (CAT) (n = 4 per group). (D) The thrombin peak and area under the curve were calculated using the manufacturer-supplied software (n = 4 for each group). Each dot represents the data from an individual mouse. Data are presented as mean ± SEM, calculated using one-way ANOVA. **p < 0.01, ****p < 0.0001.

and h*F8* KI therapies. The aPTT test evaluates early-stage coagulation function by measuring the coagulation response for 480 s, whereas the CAT assay measures overall thrombin generation through continued measurement for 120 min.[45] The aPTT test recorded 480 s in the $F8^{I22I}$ control, LNP-CRISPR, and AAV-donor groups, suggesting no improvement in the initial formation of fibrin. In contrast, the aPTT test resulted in an average of 150 ± 28 s in the AAV-LNP group, approximately 70% shorter than in the $F8^{I22I}$ control group (Figure 3B). These results showed that hFVIII production restored the initial blood-clotting ability in the AAV-LNP group. The LNP-CRISPR group was expected to have enhanced the coagulation function through the downregulation of AT; however, it did not exhibit any effect in the aPTT test, which was consistent with observations reported in the fitusiran clinical trial.[17]

The CAT assay revealed a slight improvement in thrombin generation in the LNP-CRISPR and AAV-donor groups. In contrast, the AAV-LNP group demonstrated an apparent restoration of thrombin generation (Figure 3C). The peak value for thrombin represented the capability for the maximum production of thrombin, recovering to 5.5%, 7.8%, and 35.8% of the WT value for thrombin in the LNP-CRISPR, AAV-donor, and AAV-LNP groups, respectively (Figure 3D). The area under the curve (AUC) value, which indicates the total amount of thrombin produced during CAT, recovered to 8.1%, 9.6%, and 64.8% of the WT value for AUC in the LNP-CRISPR, AAV-donor, and AAV-LNP groups, respectively (Figure 3D). These observations demonstrated that the downregulation of AT and hFVIII production in the AAV-LNP group impacted the restoration of coagulability and raised the possibility of improving the clinical symptoms of hemophilia A.

Combined use of rebalancing and hF8 KI therapies reduced bleeding lesions and prolonged survival in mice

The $F8^{I22I}$ mouse model develops spontaneous liver and lung bleeding and kidney edema.[35] Therefore, restoring blood coagulation ability through AT inhibition and hFVIII production is expected to alleviate the clinical symptoms of hemophilia. First, liver and lung tissues were embedded in paraffin, followed by the preparation of tissue slides. The bleeding frequency was calculated using the autofluorescence of red blood cells detected at a wavelength of 530 nm.[19] In the liver tissue, the AAV-LNP group exhibited a 67% reduction in bleeding frequency compared with the bleeding frequency in the $F8^{I22I}$ control group ($p < 0.001$) and recovered to the WT levels. However, spontaneous bleeding in the liver did not decrease in the LNP-CRISPR or AAV-donor groups (Figure 4A). In the lungs, the relative frequency of spontaneous bleeding decreased by 41%, 30%, and 31% in the AAV-LNP, LNP-CRISPR, and AAV-donor groups, respectively, compared with that in the $F8^{I22I}$ control group ($p = 0.012$).

Although edematous kidney lesions are not a common complication in patients with hemophilia, kidney edema was observed in the Bowman's capsule of $F8^{I22I}$ mice. As our previous study confirmed that the occurrence of edematous kidney lesions decreased with the restoration of blood coagulation ability,[19] this study also selected it as a primary criterion for assessing the recovery of blood coagulation ability. The number of edematous Bowman's capsules was estimated after hematoxylin and eosin (H&E) staining of kidney tissues. The frequency of edematous Bowman's capsules decreased by 61% in the AAV-LNP group ($p = 0.0002$), and the LNP-CRISPR group showed significantly reduced kidney edema ($p = 0.031$) (Figure 4B). Briefly, h*F8* KI into the *SerpinC1* locus induced clear clinical improvement. However, the LNP-CRISPR and AAV-donor groups seemed to show slight improvements in the lung and kidney lesions, but these improvements were insufficient.

As severe hemophilia can shorten the lifespan, the survival rate was estimated to assess the long-term therapeutic effect. During the 60-week study period, 83% of mice in the AAV-LNP group survived, whereas only 37% of mice in the $F8^{I22I}$ group survived (Figure 4C). Therefore, we concluded that the co-occurrence of low-level production of hFVIII and the downregulation of AT improved clinical symptoms, such as reduced spontaneous bleeding and prolonged survival.

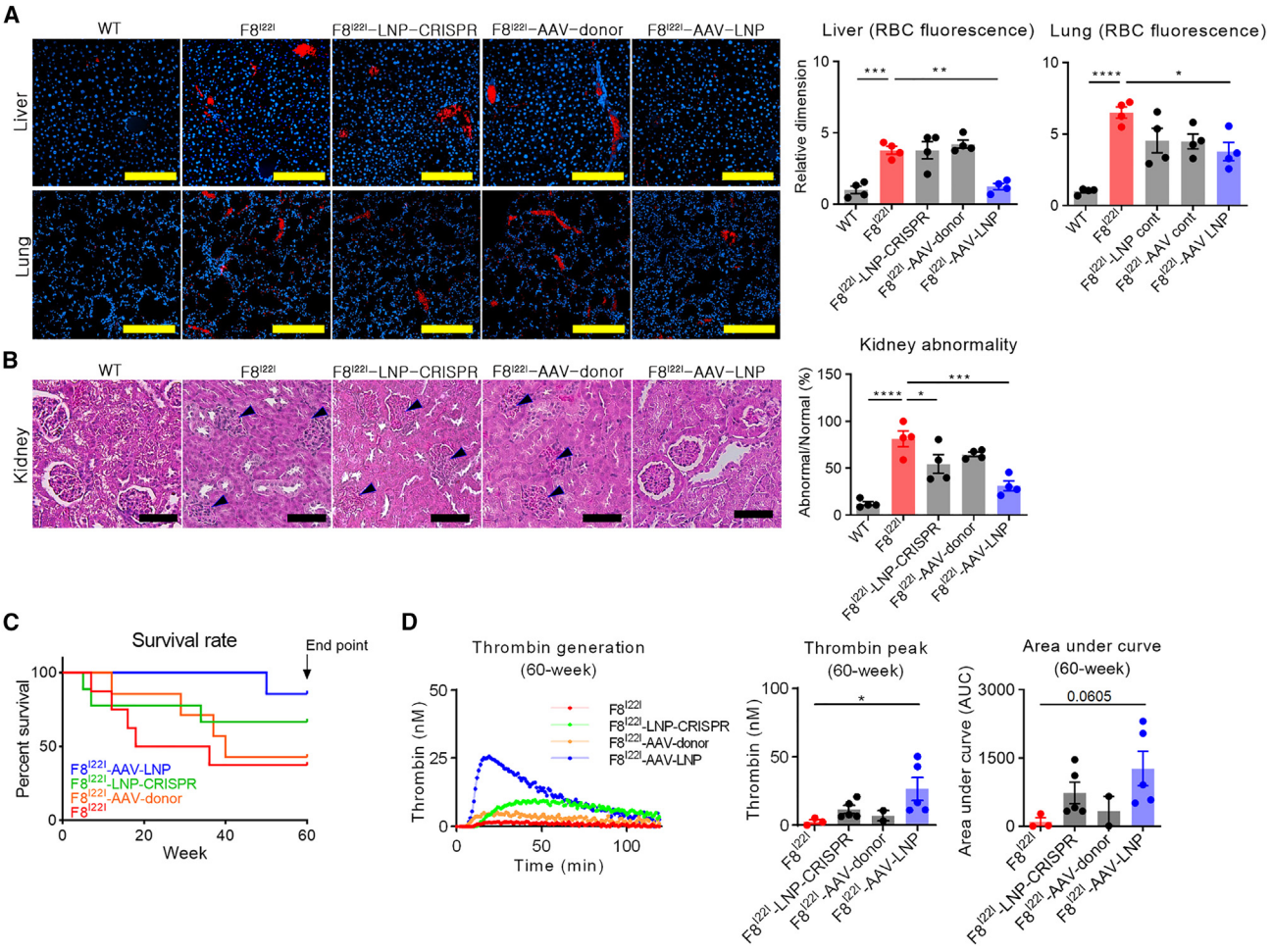

Figure 4. Improved blood coagulation activity, reduced spontaneous bleeding, and secondary complications

(A) Spontaneous bleeding was assessed in paraffin-embedded liver and lung tissues by detecting the autofluorescence signal of red blood cells (RBCs) at 530 nm. Three areas of each tissue were selected randomly from each mouse, and the dimensions of autofluorescence were calculated using ImageJ (left panel, scale bar, 200 μm). Values from each mouse were normalized to those of WT mice and subjected to RBC frequency analysis (right panel, n = 4 for each group). (B) Paraffin-embedded kidney tissues were collected to analyze hemophilic phenotypes (left panel, scale bar, 200 μm). The number of abnormally shaped glomerular capsules (black triangles) was estimated from three randomly selected areas in the cortex (right panel, n = 4 per group). Each dot represents the data from an individual mouse. Data are presented as mean ± SEM, calculated using one-way ANOVA. *$p < 0.05$, ***$p < 0.001$, ****$p < 0.0001$. (C) Survival rates were analyzed in the F8^{I22I}, LNP-CRISPR, AAV-donor, and AAV-LNP groups over 60 weeks of monitoring (F8^{I22I}, n = 8; LNP-CRISPR, n = 9; AAV-donor, n = 7; and AAV-LNP, n = 6). (D) Sustainability of therapeutic effect was assessed by CAT using 60-week follow-up mice (F8^{I22I}, n = 3; LNP-CRISPR, n = 5; AAV-donor, n = 2, AAV-LNP, n = 5). Each dot represents data from an individual mouse. Data are presented as mean ± SEM, calculated using one-way ANOVA. *$p < 0.05$.

The AAV-donor and LNP-CRISPR groups exhibited survival rates of 42% and 66%, respectively, suggesting a poor therapeutic effect in AAV-donor and a slight therapeutic effect in LNP-CRISPR. Considering the 13% decrease in blood AT concentration caused by LNP-CRISPR (Figure 2C), the improved clinical symptoms and reduced mortality in the LNP-CRISPR group appeared to develop a weak rebalancing-mediated therapeutic effect (Figure 4C). The AAV-LNP group showed a two-time reduction in blood AT concentrations compared with that in the LNP-CRISPR group; therefore, a relatively more enhanced therapeutic effect of rebalancing in the AAV-LNP group is expected.

No detectable prothrombotic events and anti-hFVIII antibody production using hF8 KI

After confirming the efficacy of *in vivo* h*F8* KI at the *SerpinC1* locus, we analyzed its safety. Although the h*F8* gene KI increased the blood coagulation ability, a cautious approach is necessary because genome editing is irreversible. As this study applied a strategy combining the rebalancing and h*F8* KI therapies, it was essential to analyze the possibility of excessive blood clotting and thrombosis, as reported in the fitusiran clinical trial.[16] Concentrations of D-dimer and thrombin-antithrombin (TAT) complexes were estimated to analyze the excessive formation of blood clots. There were no significant differences in

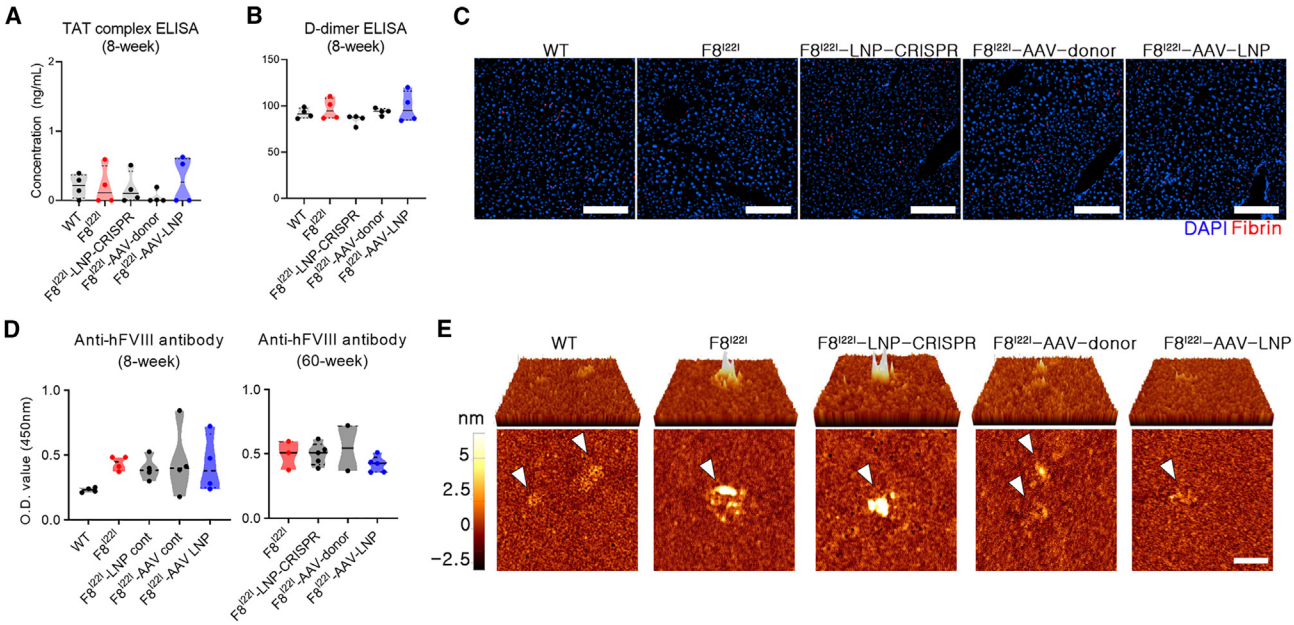

Figure 5. Undetectable prothrombotic status and the production of anti-hFVIII IgG

(A and B) Blood concentrations of thrombin-antithrombin complex (TAT) and D-dimer were measured using ELISA (n = 4 for each group). (C) The presence of fibrin clots in the liver was analyzed by immunofluorescence (scale bar, 200 μm). (D) Blood concentrations of anti-hFVIII IgG were measured by indirect ELISA using plasma samples from 8- and 60-week follow-up mice (n = 4 for each group; $F8^{I22I}$, n = 3; LNP-CRISPR, n = 5; AAV-donor, n = 2, AAV-LNP, n = 5). (E) Atomic force microscopy (AFM) images of anti-hFVIII antibody (Ab) binding to F8 in plasma. White triangle: Ab-binding agglutinations. Observations of the strong Ab-binding agglutinations are shown in elevated complex sizes (bright spots in the second and third images), which were truncated to be normal, similar to the WT results (first, fourth, and fifth images). Scale bar, 500 nm.

the levels of the D-dimer and TAT complexes in all 8-week post-injection groups of mice, including the WT and $F8^{I22I}$ controls (Figures 5A and 5B). Additionally, immunofluorescence staining for fibrin revealed no excessive fibrin clots or thrombosis in the liver (Figure 5C). Thus, our strategy, which combined the rebalancing and h*F8* KI therapies, was confirmed to be safe regarding prothrombotic effects.

One expected concern for prophylaxis is the production of inhibitors of therapeutic proteins. The development of FVIII inhibitors has been reported in approximately 30% of patients under replacement therapy, and these inhibitors have been shown to reduce the therapeutic effects.[5] Therefore, AAV-based hemophilia A gene therapy has been applied to patients without FVIII inhibitors or after the inhibitors have been eradicated by inducing immune tolerance.[46,47] Endogenous hFVIII production using the h*F8* KI was similar to that obtained using gene therapy or continuous prophylaxis. Thus, it is crucial to evaluate the formation of inhibitors of the newly generated hFVIII. The presence of anti-hFVIII antibodies in the plasma was examined using ELISA and atomic force microscopy (AFM)[48] to assess the development of hFVIII inhibitors. The $F8^{I22I}$ mice not producing hFVIII showed approximately two times higher blood anti-hFVIII immunoglobulin (Ig)G titers than those in WT mice. As hFVIII was synthesized newly in the body (AAV-donor or AAV-LNP groups), the concentration of anti-hFVIII IgG was similar to or lower in both 8- and 60-week post-injection groups, compared with that in the $F8^{I22I}$ control group (Figure 5D). Additional AFM analysis confirmed relatively strong agglutination in the $F8^{I22I}$ and LNP-CRISPR groups and moderately weaker responses in the AAV-donor and AAV-LNP groups (8 weeks post injection). This observation was similar to the inhibitor detection results obtained by ELISA (Figure 5E). In previous AAV gene therapy studies using the hemophilia A murine model, the occurrence of anti-hFVIII IgG varied based on complex differences, such as enhancer/promoter combination or AAV serotype.[49] However, low-level production of hFVIII using *in vivo* h*F8* KI did not activate the development of hFVIII inhibitors in $F8^{I22I}$ mice.

DISCUSSION

This study demonstrated the availability of *in vivo* h*F8* KI into *Serpinc1* for the combined therapy of rebalancing and hFVIII supplementation, improving blood coagulation activity and clinical symptoms. This strategy can utilize knockouts (KO or loss of function) to lower plasma concentrations of AT and KI to increase the synthesis of hFVIII. Considering the irreversible characteristics of genome-editing therapy, we combined highly efficient LNP-CRISPR and low-dose AAV as tools to induce low-level rebalancing and minimal levels of hFVIII production. Thus, we demonstrated an apparent rescue of coagulopathy and sustainable therapeutic effects *in vivo*.

In the present study, we utilized the *SerpinC1* locus as a targeted KI site. Liver sinusoidal endothelial cells are the natural site of FVIII production,[50] but *SerpinC1* is expressed in the hepatocyte. *F8* gene KI

into the *Albumin* locus showed a 2-year-long therapeutic effect,[51] and h*F8* KI into the *SerpinC1* locus showed a clinically sufficient and sustainable therapeutic effect without marked side effects. Combining *SerpinC1* targeting and h*F8* KI strategies *in vivo* has several advantages for achieving therapeutic effects. First, CRISPR-Cas9-induced DSBs at the target site followed by KO or KI could restore hemostatic function. Targeting the exon of the *SerpinC1* gene led to KO-mediated rebalancing, and KI helped in regaining the hFVIII activity, implying that all DSBs generated by CRISPR-Cas9 can be utilized to restore blood coagulation ability. Second, LNP-CRISPR can be repeatedly administered in cases of insufficient efficacy to achieve a desirable therapeutic threshold. Our previous studies demonstrated that the decrease in blood AT concentrations is proportional to the number of administrations without detectable side effects.[19] This finding implies that after recovering blood coagulation ability through rebalancing and FVIII production using a single dose of AAV-LNP, additional LNP-CRISPR administration could add a rebalancing effect in cases of insufficient hemostatic efficacy.

Previous clinical trials of fitusiran demonstrated decreased bleeding episodes with reductions in AT concentration to 70%–90% of normal values. However, side effects such as cerebral sinus thrombosis have emerged in patients with AT levels reduced by more than 85% of the normal values.[52] A subsequent phase 3 clinical trial was completed after protocol adjustment for setting the AT suppression target to 15% of normal values to address these safety concerns[53] (ClinicalTrials.gov: NCT03974113). We aimed to secure efficacy and safety by inducing a 30% downregulation of AT concentrations in blood. Despite this relatively low inhibition of AT production, we achieved an adequate hemostatic effect by compensating for approximately 10% of the FVIIIa activity through low-frequency h*F8* KI. Furthermore, there was no evidence of excessive blood clot formation or inhibitor production and a long-term sustained therapeutic effect of more than 10 months. These results suggest that our combined strategy of low-level rebalancing and therapeutic gene KI is a valid treatment option for hemophilia.

The toxicity profile of LNPs is crucial for mRNA administration using LNPs. MC3, an ionizable lipid of Onpattro, the first US Food and Drug Administration (FDA)-approved drug, has a long half-life, resulting in unexpected side effects and making it unsuitable for long-term treatment.[54] A biodegradable ester group is introduced to minimize ionizable lipid toxicity. The ester bond is hydrolyzed by esterases or lipases found in tissues or intracellular components.[54] The ester can also be hydrolyzed into alcohol and a carboxylic acid, wherein the negative charge of the carboxylate neutralizes the negative charge of the amine head or converts the amine head into a positively charged moiety such that mRNA can be released away from the lipid into the cytoplasm.[55]

Several studies have been conducted on ionizable lipids that introduce esters into the amine tail. Alnylam, the company that invented MC3, created L319 (di([Z]-non-2-en-1-yl) 9-([4-(dimethylamino) butanoyl]oxy)heptadecanedioate), a relatively more advanced version of MC3. The ionizable lipid L319 introduces an ester into the hydrophobic alkyl chain of MC3, and the hydrolyzed metabolite of L319 is water soluble and easily removed from the body.[54] Moderna Therapeutics has developed lipid 5 with an ester tail in ethanolamine. Lipid 5 has a higher protein expression efficiency than MC3 and degrades quickly in the body.[56] Ionizable lipids used in Moderna (SM-102) and Pfizer (ALC-0315) COVID-19 vaccines, approved by the FDA, are also expected to have a biodegradable effect, as they contain ester bonds. Several studies have investigated the usage of biodegradable ionizable lipids in CRISPR-Cas9 mRNA therapy. Dong et al. synthesized lipids with biodegradable esters for CRISPR-Cas9-mediated genome editing. Biodegradable lipids facilitate gene editing as they are tolerated at high doses.[57] Another study showed that a biodegradable LNP-based CRISPR-Cas9 delivery system produces >97% knockdown of serum levels of transthyretin after a single injection and that the biodegradable lipid and CRISPR-Cas9 components are transient and well tolerated *in vivo*.[58]

The AAV vectors are used widely as gene delivery tools *in vivo*; however, there are limitations in capsid-mediated immune responses and the possibility of random integration.[24,26] Notably, safety considerations for using AAVs have emerged as relatively more critical after reported deaths due to high-dose AAV gene therapy in clinical trials.[25] The AAV can induce a humoral immune response; therefore, immunomodulation has been used to diminish the immune response to AAV gene therapy.[59] AAV integration can lead to genotoxicity, and increased cancer risk is an important consideration. Transgene integration has been observed during AAV transduction in humans[60]; however, no evidence of hepatocellular carcinoma (HCC) associated with AAV integration has been reported in humans.[26] However, AAV integrated into the Rian locus has been shown to lead to HCC development in a murine liver injury model.[61] Another study showed a positive correlation between the random integration of AAV and intracellular vector copy number.[62] Thus, low-dose AAV may be a practical strategy for reducing random integration and mitigating other side effects. This study utilized AAV as a gene donor for targeted integration rather than for the episomal expression of a transgene. We induced sufficient levels of FVIII activity using a low-dose AAV, which was 30–60 times lower than that used in conventional gene therapy for hemophilia (ClinicalTrials.gov: NCT02576795, NCT03061201). Furthermore, this study utilized recombinant AAV (rAAV), which does not contain a separate promoter sequence; therefore, unexpected random AAV integration would not markedly increase the expression of a specific gene.

Genome editing is a notable option for sustainable therapy of severe genetic or chronic diseases. Intellia Therapeutics demonstrated the therapeutic potential of an *in vivo* KO strategy using CRISPR-Cas9 for Transthyretin amyloidosis[63] (ClinicalTrials.gov: NCT04601051). However, this KO or protein reduction strategy may not be suitable for treating all genetic diseases. The therapeutic gene KI strategy could be relatively more effective for treating protein-deficiency genetic disorders, including hemophilia A. Non-viral vectors are effective for preventing genotoxicity *in vivo* in therapeutic gene KI but

exhibit a limitation in that they cannot deliver DNA templates into the cell nucleus with intact nuclear envelopes. Therefore, combining viral and non-viral vectors could be an acceptable approach for conducting *in vivo* gene KI. Viral and non-viral vector-mediated delivery of genome-editing materials has advantages over existing *in vivo* KI strategies using dual or triple AAVs. First, the total amount of AAVs injected is reduced because the vector is delivered to the cell nucleus without the transduction interference that occurs when multiple AAVs are used. Second, CRISPR-Cas9 synthesized by LNP-packed Cas9 mRNA works rapidly and disappears quickly, minimizing the immune response and unintended off-target editing. Third, it enables organ-specific genome editing by matching AAV tropism with LNP targeting.

This study attempted to reduce the viral dose to minimize the adverse effects caused by AAV and used LNP instead of other viral vectors to deliver the CRISPR system. Despite strategies using low-dose AAV, a weak improvement of CAT and FVIIIa was measured in the AAV-donor group. It remains unclear whether it was caused by AAV random integration or ITR-mediated expression. The DSBs generated using CRISPR-Cas9 are not perfectly precise. This leads to unpredictable off-target events, which we confirmed were undetectable in previous study,[19] and did not analyze in this study. Therefore, such as whole genome sequencing or linear amplification-mediated PCR should be performed to accurately analyze in further study. Nevertheless, genome editing is a valuable treatment option as it can sustain long-term therapeutic effects by eliminating problematic genes or supplementing deficient proteins. Therefore, developing a novel technology that can deliver a donor DNA template to the nucleus of a quiescent cell using a non-viral vector or a safe delivery tool is needed.

In conclusion, we demonstrate a safe and sustainable genome-editing treatment using hemophilia A animal models. We combined the two existing strategies by complementing hFVIII with rebalancing, achieving a therapeutic threshold without any detectable side effects. The total AAV dose could be reduced using viral and non-viral vectors together, and an *in vivo* KI in the liver could be accomplished by AAV-mediated donor delivery and CRISPR delivery using LNPs. *In vivo* gene editing strategies could develop long-term therapeutic effects compared with those induced by gene therapy through transient gene expression; however, securing safety is relatively more important than other factors. This study provides valuable information to establish safe and long-term genome-editing-mediated treatment strategies for treating hemophilia and other protein-deficient genetic diseases.

MATERIALS AND METHODS

Recombinant AAV vector design and production

The vector for rAAV production was prepared by DNA synthesis to be an ITR-sgRNA binding sequence-homology arm-splicing acceptor-h*F8*-BDD-pA-homology arm-sgRNA binding sequence-ITR (AAV-donor). The WT h*F8* sequences were encoded with B-domain deletion. Next, ~70 μg each of the AAV-donor vector, AAV8-rep/cap plasmid, and helper plasmid was co-transfected into 1×10^8 human embryonic kidney cells of the 293T cell line using calcium phosphate. Viral particles were collected 3 days after co-transfection and purified by cesium chloride centrifugation. After titration using quantitative RT-PCR, the rAAV was stored at −80°C until use. The AAV vector preparation and recombinant AAV production steps were performed by Vector Builder (Chicago, IL, USA).

Preparation of genome-editing materials

The Cas9 mRNAs were purchased from Trilink Biotechnologies (Cat.L-7606-1000, San Diego, CA, USA). The SerpinC1 targeting sgRNAs were purchased from Axolabs (Kulmbach, Germany). The sgRNAs were chemically modified, and specific modifications of sgRNAs were described in the previous report.[64] The sequences of sgRNAs were selected through targeted deep sequencing in the previous report.[19] The sgRNAs were diluted using Tris-EDTA buffered solution (Sigma, St. Louis, MO, USA).

Preparation of LNPs

To formulate LNPs, an ethanol phase containing lipid components and an aqueous phase with RNA were combined using a microfluidic mixing device (Nanoassemblr Ignite, Precision Nanosystems, Canada). The lipid components used to formulate LNP are 244-*cis* ionizable lipids, DOPE (1,2-dioleoyl-sn-glycero-3-phosphoethanolamine), cholesterol, C16 PEG2000 ceramide (N-palmitoyl-sphingosine-1-{succinyl[methoxy(polyethylene glycol)]})2000. For the ethanol phase of the LNPs, the molar ratio of the lipid components was 244-*cis*:DOPE:cholesterol:C16-PEG ceramide = 26.5:20:52:1.5. The weight ratio of the SpCas9 mRNA to sgRNA was 1:1. The mRNAs and sgRNAs were diluted using 7.0 mM citrate with 20 mM NaCl buffer. The final volume ratio of lipids to the sum of SpCas9 mRNA and sgRNA was 1:3 and weight ratio was 10:1. The two solutions were mixed at a rate of 12 mL/min using a microfluidic device. The obtained LNPs were diluted 40 times in 1X PBS before being concentrated by ultrafiltration (Amicon Ultra-15 Centrifugal Filter Unit, UFC9010). The RiboGreen assay (ThermoFisher Scientific, Waltham, MA, USA) was used to analyze the concentration and encapsulation efficiency of the LNP. The size and PDI were measured using a DLS instrument; Zetasizer Nano ZS90 (Malvern Instruments, Malvern, UK) at 0.01 mg/mL concentration.

In vivo Luc detection

For the biodistribution analysis of LNPs, 7-week-old C57BL/6 female mice were purchased from Orient Bio, Inc. (Seongnam, Gyeonggi, Korea). The *fLuc* mRNA-loaded LNPs were administered via retro-orbital intravenous injection to mice at 0.1 mg/kg mRNA dose. Six hours later, the mice were injected intraperitoneally with 200 μL of 30 mg/mL day-luciferin (VivoGlo uLuciferin; Promega, Madison, WI, USA). Five primary organs (heart, lungs, liver, spleen, and kidney) were collected 15 min later, and luminescence was validated using an IVIS Lumina system (PerkinElmer, Waltham, MA, USA). This study was approved by the Institutional Animal Care and Use Committee at Ewha Womans University (EWHA IACUC, past-122-14). For the biodistribution analysis of AAV, 1×10^{12} vg/kg of *Luc*-encoded AAV8 was injected into 8-week-old Institute of Cancer

Research mice via the intravenous route. Two weeks after AAV transduction, a luminescent signal was detected in the live mice and their organs. This study was approved by the Institutional Biological Safety Committee (SNUIBC-P210218-4) and Institutional Animal Care and Use Committee at Seoul National University (SNU-210317-4-1), Korea.

In vivo AAV transduction and LNP injection

The C57BL/6 mice (B6, wild type; WT) were purchased from KoaTech (Pyeongtaek, Gyeonggi, Korea), whereas $F8^{I22I}$ mice were generated using CRISPR-Cas9-based gene editing.[35] Eight- to 10-week-old WT and $F8^{I22I}$ male mice were subjected to *in vivo* delivery of genetic material. The WT and $F8^{I22I}$ mice were divided randomly into the WT control, $F8^{I22I}$ control, LNP-CRISPR, AAV-donor, and AAV-LNP groups. Approximately 1×10^{12} vg/kg was injected into the AAV-donor and AAV-LNP groups, whereas 1.5 mpk of LNP-CRISPR was injected once into the LNP-CRISPR and $F8^{I22I}$-AAV-LNP groups (2 weeks after AAV-donor injection in the AAV-LNP group). Injection solution was injected via the intravenous route by mixing AAV or LNP with saline making up the final volume to 200 μL. The mice were euthanized 8 weeks after the first AAV injection to analyze the therapeutic effect. The blood and organs were collected without perfusion. The mice were maintained, with episodes of death recorded to assess the survival rate.

PCR, T7E1 analysis, and Sanger sequencing

Genomic DNA was extracted from the organ tissues using a G-DEX IIc Genomic DNA Extraction Kit (Intron Biotechnology, Gyeonggi, Korea). For indel analysis, PCR was conducted using a primer set covering DSB. The PCR amplicons were then subjected to heteroduplex hybridization and incubated with T7E1 endonuclease (New England Biolabs, Ipswich, MA, USA) for 30 min. The presence of a cut band in gel electrophoresis was designated as an indel formation. To detect the evidence of KI, a primer set that binds h*F8* and the host *SerpinC1* genome sequences was designed in the 5′ and 3′ KI expected region. After the KI PCR, the amplicons were subjected to Sanger sequencing to define the KI pattern. For HDR, KI is mediated by HA of the mouse SerpinC1 locus; therefore, sgRNA sequence in the donor template was not integrated into the DSB site. We determined by HDR that KI clones without the sgRNA binding sequences were KI. In case of HITI, a DSB occurs in the sgRNA binding site at the 5′ and 3′ ends of the AAV and host genome. Then, the donor template is integrated into the host DSB site by microhomology integration. Therefore, we determined HITI with duplicated HA and partial sgRNA sequences. The primer sequences used in this study are listed in Table S2.

Primer and probe design

Primer and probe were designed based on AAV sequences downloaded from the Nucleotide-NCBI program and aligned using SnapGene software. The aligned sequences were manually analyzed to determine the conserved region that was a suitable target. Primers and probe sequences were generated and then adjusted manually following the instructions of the Droplet Digital PCR Applications Guide (Bio-Rad). Fam- and BHQ-labeled probes were used for the amplification of the Taqman. The primer sequences used in this study are listed in Table S2.

Droplet digital PCR

For the ddPCR, Bio-Rad's QX200 ddPCR system (Bio-Rad Hercules, CA, USA) was used according to the manufacturer's instructions. The reaction was performed in a final volume of 20 μL. In particular, 10 μL of ddPCR Supermix for probes (1863026, Bio-Rad), 0.5 μL of 250 nM AAV probe (TaqMan probe labeled with Fam), 1.8 μL each of the 900 nM forward and reverse AAV primer, and DEPC-water to reach the final volume were used. Each ddPCR assay mixture was loaded into a disposable droplet generator cartridge (Bio-Rad). Then, 70 μL of droplet generation oil for probes (1863005, Bio-Rad) was loaded into each of the eight oil wells. The cartridge was then placed inside the QX200 droplet generator (Bio-Rad). When droplet generation was completed, the droplets were transferred to a ddPCR 96-well PCR plate (12001925, Bio-Rad) using a multichannel pipet. The plate was heat-scaled with foil and placed in a T100 Thermal Cycler (Bio-Rad). Thermal cycling conditions were as follows: 95°C for 10 min, then 40 cycles of 94°C for 30 s and 55°C for 1 min, and 98°C for 10 min, and a 4°C indefinite hold. After amplification, the plate was loaded on the droplet reader (Bio-Rad) and the droplets from each well of the plate were read automatically. QuantaSoft software was used to count the PCR-positive and PCR-negative droplets to provide absolute quantification of target DNA. The quantification measurements of each target were expressed as the copy number per 1 μL of reaction.

ELISA (AT, hF8, ALT, AST, TAT, D-dimer)

Approximately 450 μL of fresh blood was collected from the inferior vena cava using a syringe prefilled with 50 μL of 3.2% sodium citrate (Medicago, Durham, NC, USA), and plasma was collected after centrifugation at 3,000 × *g*. Liver tissues were collected and lysed in RIPA buffer (Intron Biotechnology) containing proteinase inhibitors, followed by protein extraction. The plasma concentrations of mouse AST, ALT, AT, human FVIII, active FVIII, TAT, and D-dimer were measured using a commercial ELISA kit following the manufacturer's instructions. Detailed information on the ELISA kits and the reaction conditions is listed in Table S3.

Western blotting

Approximately 20 μg of liver tissue proteins were separated by sodium dodecyl sulfate-polyacrylamide gel electrophoresis. The proteins were then electrotransferred onto polyvinylidene fluoride membranes (EMD Millipore, Billerica, MA, USA). The membranes were incubated in a blocking buffer (1X TBS and 5% w/v non-fat milk) for 2 h at room temperature (RT). After 16 h of incubation with the primary antibody at 4°C, the membranes were washed with Tris-PBS with 0.1% Tween 20. Immunoreactive proteins were detected using enhanced chemiluminescence (ECL kit; Abclon, Seoul, Korea) after incubation with horseradish peroxidase-conjugated secondary antibody for 1 h at RT. Information on the antibodies and conditions used in this study is provided in Table S4.

Immunofluorescence

Liver tissues were collected after anesthetization, subjected to precipitation in 15% sucrose for 6 h and 30% sucrose for 1 day, and embedded in an optimal cutting temperature compound (Sakura Finetek, Tokyo, Japan) with gradual freezing to −80°C. Approximately 15-μm-thick cryosections were prepared using a Cryostat microtome (Leica, Wetzler, Germany). Immunofluorescence analysis for detecting hFVIII was conducted by incubating the cryosections with primary antibodies at 4°C overnight, followed by incubation with corresponding secondary antibodies. Expression of hFVIII was detected using Cytation 5 Cell Imaging Multi-Mode Reader (BioTek, Winooski, VT, USA). Information on the antibodies and conditions used in this study is provided in Table S4.

Measurement of FVIII activity

The activity of FVIII in blood was measured using a Factor VIIIa Activity Assay Kit (Abcam, Waltham, MA, USA). Briefly, 10.0 μL of diluted plasma, enzymes I and II from the kit, and phospholipids were mixed and incubated for 15 min at 37°C in 96-well plates, and then, 2.0 μL of FXa substrate-AMC was added into each well. Next, fluorescence intensity (excitation/emission = 360/450 nm) was measured every 2 min for 60 min at 37°C using Cytation 5 Cell Imaging Multi-Mode Reader (BioTek), and FVIII activity was estimated by applying the measured fluorescence values to the standard curve of FVIII activity.

Analysis of aPTT and CAT

For aPTT analysis, approximately 30 μL of plasma collected from mice and 30 μL of the aPTT reagent (Thermo Fisher Scientific) were mixed in each well of a 96-well microplate and incubated at 37°C for 5 min. Next, 30 μL of 26 μM calcium chloride was added to each well. Absorbance was measured at 405 nm every 10 s for 8 min after shaking for the first 10 s using a Tecan Sunrise Microplate Reader (Tecan, Männedorf, Switzerland). The delta optical density (ΔOD, i.e., OD value of each time point − OD value 10 s ago) was calculated, and the time point with the highest ΔOD value was designated as the aPTT. The CAT experiment measured thrombin generation activity using the Technothrombin TGA kit (Diapharma, West Chester Township, OH, USA). A reaction mix, comprising 10 μL of reagent C low buffer, 50 μL of the substrate, and 40 μL of diluted plasma, was added to each well of a 96-well plate. Fluorescence intensities were measured for 120 min at 1-min intervals using Cytation 5 Cell Imaging Multi-Mode Reader (BioTek). The thrombin generation curves, peak heights, and peak times were determined using the software provided by the manufacturer (Diapharma).

Histological analyses

Liver, lung, and kidney tissues were fixed in a 4% paraformaldehyde solution (Thermo Fisher Sientific). For H&E staining, deparaffinized tissues were stained with 0.1% Mayer's H&E solution. The deparaffinized liver and lung tissues slides were stained using 4′, 6-diamidino-2-phenylindole (Thermo Fisher Scientific) to detect bleeding lesions and fluorescence signals were detected at 530-nm wavelengths using Cytation 5 Cell Imaging Multi-Mode Reader (BioTeK). All images were converted to 8-bit grayscale, and the total fluorescence signals were measured using ImageJ software, as described previously.[19]

Anti-hFVIII antibody detection

For the indirect ELISA experiment, 96-well microplates were coated using recombinant hFVIII (Prospec Bio, Rehovot, Israel) at 1.0 μg/mL in PBS overnight at 4°C. After washing and blocking using 5% skimmed milk for 2 h at RT, 100 μL of diluted plasma was added and incubated for 2 h at RT. Next, horseradish peroxidase-conjugated goat anti-mouse IgG antibody (Thermo Fisher Scientific) was added and incubated for 1 h at RT. The 3,3′,5,5′-tetramethylbenzidine was used as a substrate, followed by a comparison of the OD values measured at 459 nm for each group.

Atomic force microscopy

Dry-state tapping mode AFM (NX-10; Park Systems, Suwon, Korea) imaging was performed to visualize the presence of anti-hFVIII antibodies. For sample preparations, 20 μL of the sample was dropped onto a freshly cleaned silicon substrate and then air-dried for 5 min. The deposited sample surfaces were washed twice with distilled water. AFM imaging was performed using a silicon SPM cantilever (NCHR-50, Nanosensors, Neuchatel, Switzerland) with a resonance frequency of 320 kHz. The scan rate for each image was set to 0.7 Hz. The XEI program was used to analyze the AFM images.

Statistical analyses

Statistical analyses were performed using the unpaired Student's t test, one-way analysis of variance, and Kaplan-Meier survival analysis in GraphPad Prism (Version 9.5.1; GraphPad, San Diego, CA, USA). Statistical significance was set at $p < 0.05$.

DATA AND CODE AVAILABILITY

The data of the current study are available from the corresponding author upon reasonable request.

SUPPLEMENTAL INFORMATION

Supplemental information can be found online at https://doi.org/10.1016/j.omtn.2023.102050.

ACKNOWLEDGMENTS

Supported by the National Research Foundation of Korea (2021R1I1A2044117), Korea Institute of Toxicology (1711133848), Ministry of Food and Drug Safety (21173MFDS562), and Bio & Medical Technology Development Program of the National Research Foundation.

Funded by the Ministry of Science, ICT & Future Planning (2019M3A9H1103786 and 2022M3E5F1081328).

AUTHOR CONTRIBUTIONS

J.P.H. and Y.L. drafted the manuscript and performed the experiments. J.H.L. performed blood coagulation experiments. H.Y.C. and G.S.L. performed histological analysis. M.C. and K.M. performed the droplet digital PCR. Y.R.N. and Haeshin Lee performed atomic

force microscopy. Hyukjin Lee and S.C.Y. supervised and designed the study.

DECLARATION OF INTERESTS

Hyukjin Lee received a research grant from ST Pharm, and ST Pharm also has a license for certain intellectual property invented at Ewha Womans University.

REFERENCES

1. Berntorp, E., and Shapiro, A.D. (2012). Modern haemophilia care. Lancet *379*, 1447–1456.
2. Makris, M. (2012). Prophylaxis in haemophilia should be life-long. Blood Transfus *10*, 165–168.
3. Tiede, A. (2015). Half-life extended factor VIII for the treatment of hemophilia A. J. Thromb. Haemostasis *13*, S176–S179.
4. Malec, L.M., Cheng, D., Witmer, C.M., Jaffray, J., Kouides, P.A., Haley, K.M., Sidonio, R.F., Jr., Johnson, K., Recht, M., White, G., et al. (2020). The impact of extended half-life factor concentrates on prophylaxis for severe hemophilia in the United States. Am. J. Hematol. *95*, 960–965.
5. Volkers, P., Hanschmann, K.M., Calvez, T., Chambost, H., Collins, P.W., Demiguel, V., Hart, D.P., Hay, C.R.M., Goudemand, J., Ljung, R., et al. (2019). Recombinant factor VIII products and inhibitor development in previously untreated patients with severe haemophilia A: Combined analysis of three studies. Haemophilia *25*, 398–407.
6. Kempton, C.L., and Meeks, S.L. (2014). Toward optimal therapy for inhibitors in hemophilia. Blood *124*, 3365–3372.
7. Morfini, M., Haya, S., Tagariello, G., Pollmann, H., Quintana, M., Siegmund, B., Stieltjes, N., Dolan, G., and Tusell, J. (2007). European study on orthopaedic status of haemophilia patients with inhibitors. Haemophilia *13*, 606–612.
8. Pipe, S.W., Gonen-Yaacovi, G., and Segurado, O.G. (2022). Hemophilia A gene therapy: current and next-generation approaches. Expet Opin. Biol. Ther. *22*, 1099–1115.
9. Ellsworth, P., and Ma, A. (2021). Factor-mimetic and rebalancing therapies in hemophilia A and B: the end of factor concentrates? Hematol. Am. Soc. Hematol. Educ. Program *2021*, 219–225.
10. Rogers, G.L., and Herzog, R.W. (2015). Gene therapy for hemophilia. Front. Biosci. *20*, 556–603.
11. Pasi, K.J., Rangarajan, S., Mitchell, N., Lester, W., Symington, E., Madan, B., Laffan, M., Russell, C.B., Li, M., Pierce, G.F., and Wong, W.Y. (2020). Multiyear Follow-up of AAV5-hFVIII-SQ Gene Therapy for Hemophilia A. N. Engl. J. Med. *382*, 29–40.
12. Kessler, P.D., Podsakoff, G.M., Chen, X., McQuiston, S.A., Colosi, P.C., Matelis, L.A., Kurtzman, G.J., and Byrne, B.J. (1996). Gene delivery to skeletal muscle results in sustained expression and systemic delivery of a therapeutic protein. Proc. Natl. Acad. Sci. USA *93*, 14082–14087.
13. Weyand, A.C., and Pipe, S.W. (2019). New therapies for hemophilia. Blood *133*, 389–398.
14. Chowdary, P. (2020). Anti-tissue factor pathway inhibitor (TFPI) therapy: a novel approach to the treatment of haemophilia. Int. J. Hematol. *111*, 42–50.
15. Polderdijk, S.G.I., Baglin, T.P., and Huntington, J.A. (2017). Targeting activated protein C to treat hemophilia. Curr. Opin. Hematol. *24*, 446–452.
16. Pasi, K.J., Rangarajan, S., Georgiev, P., Mant, T., Creagh, M.D., Lissitchkov, T., Bevan, D., Austin, S., Hay, C.R., Hegemann, I., et al. (2017). Targeting of Antithrombin in Hemophilia A or B with RNAi Therapy. N. Engl. J. Med. *377*, 819–828.
17. Pasi, K.J., Lissitchkov, T., Mamonov, V., Mant, T., Timofeeva, M., Bagot, C., Chowdary, P., Georgiev, P., Gercheva-Kyuchukova, L., Madigan, K., et al. (2021). Targeting of antithrombin in hemophilia A or B with investigational siRNA therapeutic fitusiran - results of the phase 1 inhibitor cohort. J. Thromb. Haemostasis *19*, 1436–1446.
18. Ran, F.A., Hsu, P.D., Wright, J., Agarwala, V., Scott, D.A., and Zhang, F. (2013). Genome engineering using the CRISPR-Cas9 system. Nat. Protoc. *8*, 2281–2308.
19. Han, J.P., Kim, M., Choi, B.S., Lee, J.H., Lee, G.S., Jeong, M., Lee, Y., Kim, E.A., Oh, H.K., Go, N., et al. (2022). In vivo delivery of CRISPR-Cas9 using lipid nanoparticles enables antithrombin gene editing for sustainable hemophilia A and B therapy. Sci. Adv. *8*, eabj6901.
20. Chen, H., Shi, M., Gilam, A., Zheng, Q., Zhang, Y., Afrikanova, I., Li, J., Gluzman, Z., Jiang, R., Kong, L.-J., and Chen-Tsai, R.Y. (2019). Hemophilia A ameliorated in mice by CRISPR-based in vivo genome editing of human Factor VIII. Sci. Rep. *9*, 16838.
21. Lee, J.H., Oh, H.K., Choi, B.S., Lee, H.H., Lee, K.J., Kim, U.G., Lee, J., Lee, H., Lee, G.S., Ahn, S.J., et al. (2022). Genome editing-mediated knock-in of therapeutic genes ameliorates the disease phenotype in a model of hemophilia. Mol. Ther. Nucleic Acids *29*, 551–562.
22. Gaj, T., Staahl, B.T., Rodrigues, G.M.C., Limsirichai, P., Ekman, F.K., Doudna, J.A., and Schaffer, D.V. (2017). Targeted gene knock-in by homology-directed genome editing using Cas9 ribonucleoprotein and AAV donor delivery. Nucleic Acids Res. *45*, e98.
23. He, X., Zhang, Z., Xue, J., Wang, Y., Zhang, S., Wei, J., Zhang, C., Wang, J., Urip, B.A., Ngan, C.C., et al. (2022). Low-dose AAV-CRISPR-mediated liver-specific knock-in restored hemostasis in neonatal hemophilia B mice with subtle antibody response. Nat. Commun. *13*, 7275.
24. Ronzitti, G., Gross, D.A., and Mingozzi, F. (2020). Human Immune Responses to Adeno-Associated Virus (AAV) Vectors. Front. Immunol. *11*, 670.
25. (2020). High-dose AAV gene therapy deaths. Nat. Biotechnol. *38*, 910.
26. Sabatino, D.E., Bushman, F.D., Chandler, R.J., Crystal, R.G., Davidson, B.L., Dolmetsch, R., Eggan, K.C., Gao, G., Gil-Farina, I., Kay, M.A., et al. (2022). Evaluating the state of the science for adeno-associated virus integration: An integrated perspective. Mol. Ther. *30*, 2646–2663.
27. Cheng, Q., Wei, T., Farbiak, L., Johnson, L.T., Dilliard, S.A., and Siegwart, D.J. (2020). Selective organ targeting (SORT) nanoparticles for tissue-specific mRNA delivery and CRISPR-Cas gene editing. Nat. Nanotechnol. *15*, 313–320.
28. Pardi, N., Tuyishime, S., Muramatsu, H., Kariko, K., Mui, B.L., Tam, Y.K., Madden, T.D., Hope, M.J., and Weissman, D. (2015). Expression kinetics of nucleoside-modified mRNA delivered in lipid nanoparticles to mice by various routes. J. Control Release *217*, 345–351.
29. Kim, M., Jeong, M., Lee, G., Lee, Y., Park, J., Jung, H., Im, S., Yang, J.S., Kim, K., and Lee, H. (2023). Novel piperazine-based ionizable lipid nanoparticles allow the repeated dose of mRNA to fibrotic lungs with improved potency and safety. Bioeng. Transl. Med.
30. Klamroth, R., Windyga, J., Radulescu, V., Collins, P.W., Stasyshyn, O., Ibrahim, H.M., Engl, W., Tangada, S.D., Savage, W., and Ewenstein, B. (2021). Rurioctocog alfa pegol PK-guided prophylaxis in hemophilia A: results from the phase 3 PROPEL study. Blood *137*, 1818–1827.
31. Peters, R., and Harris, T. (2018). Advances and innovations in haemophilia treatment. Nat. Rev. Drug Discov. *17*, 493–508.
32. Yao, X., Wang, X., Hu, X., Liu, Z., Liu, J., Zhou, H., Shen, X., Wei, Y., Huang, Z., Ying, W., et al. (2017). Homology-mediated end joining-based targeted integration using CRISPR/Cas9. Cell Res. *27*, 801–814.
33. Dilliard, S.A., Cheng, Q., and Siegwart, D.J. (2021). On the mechanism of tissue-specific mRNA delivery by selective organ targeting nanoparticles. Proc. Natl. Acad. Sci. USA *118*, e2109256118.
34. Akinc, A., Querbes, W., De, S., Qin, J., Frank-Kamenetsky, M., Jayaprakash, K.N., Jayaraman, M., Rajeev, K.G., Cantley, W.L., Dorkin, J.R., et al. (2010). Targeted delivery of RNAi therapeutics with endogenous and exogenous ligand-based mechanisms. Mol. Ther. *18*, 1357–1364.
35. Han, J.P., Song, D.W., Lee, J.H., Lee, G.S., and Yeom, S.C. (2021). Novel Severe Hemophilia A Mouse Model with Factor VIII Intron 22 Inversion. Biology *10*, 704.
36. Han, J.P., Chang, Y.J., Song, D.W., Choi, B.S., Koo, O.J., Yi, S.Y., Park, T.S., and Yeom, S.C. (2020). High Homology-Directed Repair Using Mitosis Phase and Nucleus Localizing Signal. Int. J. Mol. Sci. *21*, 3747.
37. Lin, S., Staahl, B.T., Alla, R.K., and Doudna, J.A. (2014). Enhanced homology-directed human genome engineering by controlled timing of CRISPR/Cas9 delivery. Elife *3*, e04766.
38. Li, M., Zhou, X., Mei, J., Geng, X., Zhou, Y., Zhang, W., and Xu, C. (2014). Study on the activity of the signaling pathways regulating hepatocytes from G0 phase into G1 phase during rat liver regeneration. Cell. Mol. Biol. Lett. *19*, 181–200.

39. Daya, S., and Berns, K.I. (2008). Gene therapy using adeno-associated virus vectors. Clin. Microbiol. Rev. *21*, 583–593.

40. Wang, J., Xie, J., Lu, H., Chen, L., Hauck, B., Samulski, R.J., and Xiao, W. (2007). Existence of transient functional double-stranded DNA intermediates during recombinant AAV transduction. Proc. Natl. Acad. Sci. USA *104*, 13104–13109.

41. Ozelo, M.C., Mahlangu, J., Pasi, K.J., Giermasz, A., Leavitt, A.D., Laffan, M., Symington, E., Quon, D.V., Wang, J.D., Peerlinck, K., et al. (2022). Valoctocogene Roxaparvovec Gene Therapy for Hemophilia A. N. Engl. J. Med. *386*, 1013–1025.

42. Hanlon, K.S., Kleinstiver, B.P., Garcia, S.P., Zaborowski, M.P., Volak, A., Spirig, S.E., Muller, A., Sousa, A.A., Tsai, S.Q., Bengtsson, N.E., et al. (2019). High levels of AAV vector integration into CRISPR-induced DNA breaks. Nat. Commun. *10*, 4439.

43. Jenkins, P.V., Collins, P.W., Goldman, E., McCraw, A., Riddell, A., Lee, C.A., and Pasi, K.J. (1994). Analysis of intron 22 inversions of the factor VIII gene in severe hemophilia A: implications for genetic counseling. Blood *84*, 2197–2201.

44. Earley, L.F., Conatser, L.M., Lue, V.M., Dobbins, A.L., Li, C., Hirsch, M.L., and Samulski, R.J. (2020). Adeno-Associated Virus Serotype-Specific Inverted Terminal Repeat Sequence Role in Vector Transgene Expression. Hum. Gene Ther. *31*, 151–162.

45. Duarte, R.C.F., Ferreira, C.N., Rios, D.R.A., Reis, H.J.D., and Carvalho, M.D.G. (2017). Thrombin generation assays for global evaluation of the hemostatic system: perspectives and limitations. Rev. Bras. Hematol. Hemoter. *39*, 259–265.

46. Blair, H.A. (2022). Valoctocogene Roxaparvovec: First Approval. Drugs *82*, 1505–1510.

47. Nakar, C., and Shapiro, A. (2019). Hemophilia A with inhibitor: Immune tolerance induction (ITI) in the mirror of time. Transfus. Apher. Sci. *58*, 578–589.

48. Hu, J., Gao, M., Wang, Z., Chen, Y., Song, Z., and Xu, H. (2021). Direct imaging of antigen-antibody binding by atomic force microscopy. Appl. Nanosci. *11*, 293–300.

49. Greig, J.A., Wang, Q., Reicherter, A.L., Chen, S.J., Hanlon, A.L., Tipper, C.H., Clark, K.R., Wadsworth, S., Wang, L., and Wilson, J.M. (2017). Characterization of Adeno-Associated Viral Vector-Mediated Human Factor VIII Gene Therapy in Hemophilia A Mice. Hum. Gene Ther. *28*, 392–402.

50. Do, H., Healey, J.F., Waller, E.K., and Lollar, P. (1999). Expression of factor VIII by murine liver sinusoidal endothelial cells. J. Biol. Chem. *274*, 19587–19592.

51. Zhang, J.P., Cheng, X.X., Zhao, M., Li, G.H., Xu, J., Zhang, F., Yin, M.D., Meng, F.Y., Dai, X.Y., Fu, Y.W., et al. (2019). Curing hemophilia A by NHEJ-mediated ectopic F8 insertion in the mouse. Genome Biol. *20*, 276.

52. Gualtierotti, R., Pasca, S., Ciavarella, A., Arcudi, S., Giachi, A., Garagiola, I., Suffritti, C., Siboni, S.M., and Peyvandi, F. (2022). Updates on Novel Non-Replacement Drugs for Hemophilia. Pharmaceuticals *15*, 1183.

53. Nogami, K., and Shima, M. (2023). Current and future therapies for haemophilia-Beyond factor replacement therapies. Br. J. Haematol. *200*, 23–34.

54. Maier, M.A., Jayaraman, M., Matsuda, S., Liu, J., Barros, S., Querbes, W., Tam, Y.K., Ansell, S.M., Kumar, V., Qin, J., et al. (2013). Biodegradable lipids enabling rapidly eliminated lipid nanoparticles for systemic delivery of RNAi therapeutics. Mol. Ther. *21*, 1570–1578.

55. Prata, C.A.H., Zhao, Y., Barthelemy, P., Li, Y., Luo, D., McIntosh, T.J., Lee, S.J., and Grinstaff, M.W. (2004). Charge-reversal amphiphiles for gene delivery. J. Am. Chem. Soc. *126*, 12196–12197.

56. Sabnis, S., Kumarasinghe, E.S., Salerno, T., Mihai, C., Ketova, T., Senn, J.J., Lynn, A., Bulychev, A., McFadyen, I., Chan, J., et al. (2018). A Novel Amino Lipid Series for mRNA Delivery: Improved Endosomal Escape and Sustained Pharmacology and Safety in Non-human Primates. Mol. Ther. *26*, 1509–1519.

57. Zhang, X., Li, B., Luo, X., Zhao, W., Jiang, J., Zhang, C., Gao, M., Chen, X., and Dong, Y. (2017). Biodegradable Amino-Ester Nanomaterials for Cas9 mRNA Delivery in Vitro and in Vivo. ACS Appl. Mater. Interfaces *9*, 25481–25487.

58. Finn, J.D., Smith, A.R., Patel, M.C., Shaw, L., Youniss, M.R., van Heteren, J., Dirstine, T., Ciullo, C., Lescarbeau, R., Seitzer, J., et al. (2018). A Single Administration of CRISPR/Cas9 Lipid Nanoparticles Achieves Robust and Persistent In Vivo Genome Editing. Cell Rep. *22*, 2227–2235.

59. Chu, W.S., and Ng, J. (2021). Immunomodulation in Administration of rAAV: Preclinical and Clinical Adjuvant Pharmacotherapies. Front. Immunol. *12*, 658038.

60. Fong, S., Yates, B., Sihn, C.R., Mattis, A.N., Mitchell, N., Liu, S., Russell, C.B., Kim, B., Lawal, A., Rangarajan, S., et al. (2022). Interindividual variability in transgene mRNA and protein production following adeno-associated virus gene therapy for hemophilia A. Nat. Med. *28*, 789–797.

61. Dalwadi, D.A., Torrens, L., Abril-Fornaguera, J., Pinyol, R., Willoughby, C., Posey, J., Llovet, J.M., Lanciault, C., Russell, D.W., Grompe, M., and Naugler, W.E. (2021). Liver Injury Increases the Incidence of HCC following AAV Gene Therapy in Mice. Mol. Ther. *29*, 680–690.

62. Nguyen, G.N., Everett, J.K., Kafle, S., Roche, A.M., Raymond, H.E., Leiby, J., Wood, C., Assenmacher, C.A., Merricks, E.P., Long, C.T., et al. (2021). A long-term study of AAV gene therapy in dogs with hemophilia A identifies clonal expansions of transduced liver cells. Nat. Biotechnol. *39*, 47–55.

63. Gillmore, J.D., Maitland, M.L., and Lebwohl, D. (2021). CRISPR-Cas9 In Vivo Gene Editing for Transthyretin Amyloidosis. Reply. N. Engl. J. Med. *385*, 1722–1723.

64. Yin, H., Song, C.Q., Suresh, S., Wu, Q., Walsh, S., Rhym, L.H., Mintzer, E., Bolukbasi, M.F., Zhu, L.J., Kauffman, K., et al. (2017). Structure-guided chemical modification of guide RNA enables potent non-viral in vivo genome editing. Nat. Biotechnol. *35*, 1179–1187.